

Scalpel: Fine-Grained Alignment of Attention Activation Manifolds via Mixture Gaussian Bridges to Mitigate Multimodal Hallucination

Ziqiang Shi^{**}, Ruijie Liu^{*}, Shanshan Yu[†], Satoshi Munakata[†], Koichi Shirahata[†]

^{*} Fujitsu Research & Development Center Co.,LTD., Beijing, China

[†] Fujitsu Limited, Tokyo, Japan

Abstract

Rapid progress in large vision-language models (LVLMs) has achieved unprecedented performance in vision-language tasks. However, due to the strong prior of large language models (LLMs) and misaligned attention across modalities, LVLMs often generate outputs inconsistent with visual content - termed hallucination. To address this, we propose Scalpel, a method that reduces hallucination by refining attention activation distributions toward more credible regions. Scalpel predicts trusted attention directions for each head in Transformer layers during inference and adjusts activations accordingly. It employs a Gaussian mixture model to capture multi-peak distributions of attention in trust and hallucination manifolds, and uses entropic optimal transport (equivalent to Schrödinger bridge problem) to map Gaussian components precisely. During mitigation, Scalpel dynamically adjusts intervention strength and direction based on component membership and mapping relationships between hallucination and trust activations. Extensive experiments across multiple datasets and benchmarks demonstrate that Scalpel effectively mitigates hallucinations, outperforming previous methods and achieving state-of-the-art performance. Moreover, Scalpel is model- and data-agnostic, requiring no additional computation, only a single decoding step.

1. Introduction

Large visual language models (LVLMs) have become essential tools for handling diverse visual tasks and performing complex visual question-answering due to their strong capabilities in content understanding and generation [19, 33, 36, 40]. Despite these advancements, LVLMs often suffer from the “hallucination” problem, where generated text appears plausible but misaligns with image content or even fabricates elements not present in the input [10, 14, 14, 20, 27, 29, 37]. This issue significantly un-

dermines their reliability in critical domains such as health-care, autonomous driving, and security monitoring.

The hallucinations in current LVLMs are generally attributed to two main factors: the strong language priors inherited from pre-trained large language models (LLMs) [14, 20], and the model’s tendency to over-attend to irrelevant visual tokens or system tokens unrelated to the given instruction [27, 29, 34, 37]. To mitigate this, researchers have explored reinforcement learning (RL) strategies that fine-tune LVLMs using high-quality [5, 20, 21, 27], hallucination-free feedback—either human-labeled or AI-generated—to improve alignment between vision and language while reducing reliance on LLM priors. However, these methods demand substantial computational resources for annotation and training, making them impractical in resource-constrained environments. Consequently, recent studies have shifted focus toward inference-time optimization techniques that do not require retraining, such as contrastive decoding [8, 10, 14, 35], which reduces hallucinations by adjusting logit scores. Although training-free, these methods still fall short in effectiveness and often introduce noticeable latency due to multi-step decoding.

While both approaches yield some success, they rarely investigate the internal mechanisms of the LVLM itself to uncover the root causes of hallucinations. In contrast, this paper delves into the role of attention activation across different heads and layers within the LVLM’s Transformer [31] architecture during the generation of hallucinated content. We discover that individual attention heads contribute differently to hallucinations. By precisely identifying those responsible and applying targeted interventions, we can significantly enhance output quality and multimodal reasoning performance.

Our key contributions are summarized as follows:

- We propose Scalpel, a novel, training-free, plug-and-play method that enables customized correction of attention activations at the token level without compromising the LLM’s knowledge capacity, effectively reducing hallucinations in LVLMs.
- To achieve precise attention correction per token, Scalpel

^{**}Corresponding author: shiziqiang@fujitsu.com

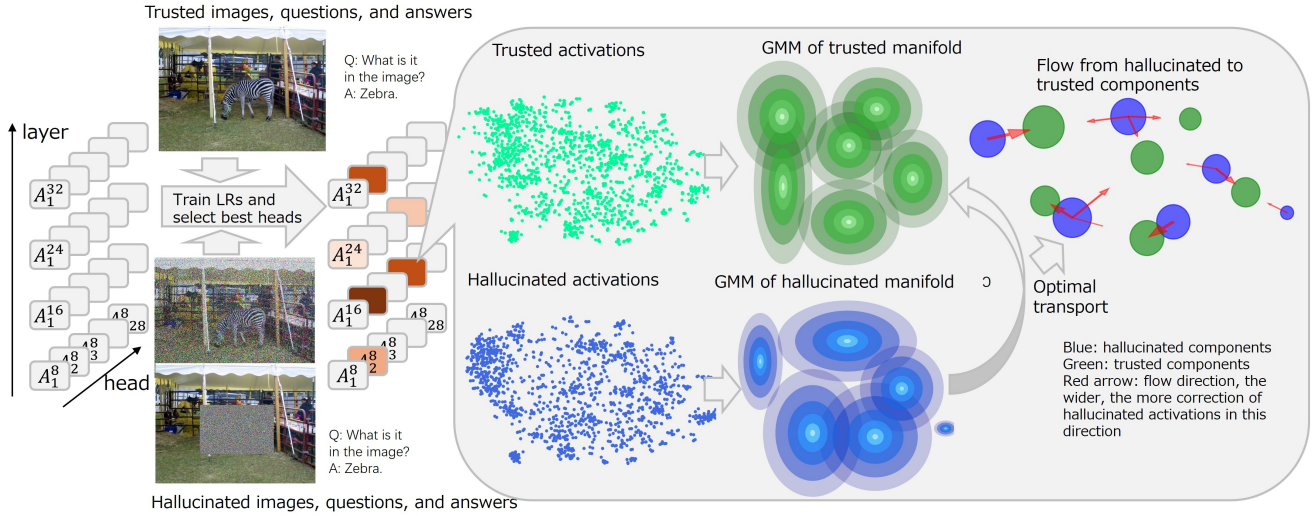


Figure 1. Schematic diagram illustrating the principle of the Scalpel method. First, the trusted and hallucinated attention activations of all heads are obtained by inputting both correct and hallucinated data into the LVLM. These activations serve two purposes. The first is to identify the heads with the highest hallucination discrimination capability using a classifier. The second is to analyze the distribution of credible and hallucinated attention activations across tokens, thereby determining the influence of each individual token on each head.

employs Gaussian mixture models (GMMs) to represent trusted and hallucinated attention activation manifolds, then applies Schrödinger bridge problem solving theory to compute optimal transport between these GMMs as shown in Figure 1. This allows for component-specific correction based on the current token’s activation.

- Experimental results on POPE [17] and MME [9] benchmarks demonstrate that Scalpel significantly improves performance on LLaVA-1.5 [19] and Qwen2.5-VL [2], proving its model-agnostic and task-agnostic applicability across multiple databases.

2. Related Work

2.1. Hallucination in LVLMs

Although LVLMs, built upon open-source language models such as LLaMA [28] and Vicuna [7], have achieved effective multimodal fusion of text and images—greatly enhancing cross-modal understanding and generation—they still face a critical challenge: hallucination. Hallucination refers to factual inconsistencies between the generated text and the input image, often manifesting as fabricated objects or inaccurate descriptions of attributes and relationships. This issue primarily stems from two key factors: (1) an over-reliance on prior knowledge (e.g., biases in training data or inherent language priors within LLMs) [14, 20], and (2) limitations in visual encoder localization, misalignment of multimodal information [27, 34], or suboptimal attention modeling during decoding [29, 37], all of which hinder accurate associations between inputs and outputs.

2.2. Hallucination Mitigation in LVLMs

LVLM hallucination mitigation falls into two categories: training-based and training-free post-processing methods. Training-based approaches include: MIA-DPO [20] creates multi-image data via grid collages from single inputs; LLaVA-RLHF [27] reduces reward hacking through fact-grounded reward models; DAMA [21] dynamically optimizes training by aligning data difficulty with response strategies; PerturboLLAVA [5] weakens language prior reliance via adversarial text perturbations; EACO [34] achieves alignment with only 5,000 images (high efficiency); AMP [38] enhances fine-grained recognition through multi-level preference optimization.

Training-free post-processing improves generation accuracy without retraining. These methods fall into two categories: contrastive decoding [8, 10, 14, 35] and attention reallocation [29, 35, 37, 39]. Contrastive decoding reduces bias via cross-image comparison (VCD [14]), uses penalties/rollback for refinement (OPERA [10]), and strengthens vision-language alignment (M3ID [8]). Attention reallocation improves responsiveness with blind-token calibration (AVISC [35]), provides plug-and-play enhancement (ClearSight [37]), optimizes resource use through recycling (AttnReal [29]), and broadcasts attention matrices for focus enhancement (EAH [39]), achieving minimal computational overhead.

Our approach fundamentally differs by leveraging inference-time intervention [6, 16]. The core procedure comprises: (1) identifying factual-response directions in ac-

tivation space; (2) steering activation vectors toward these directions during reasoning. Compared to existing methods, this technique offers: negligible computational overhead; strong interpretability through explicit activation manipulation; and significant hallucination reduction while preserving generation quality.

3. Methodology

3.1. Background and Notation

The input to an LVLM is multimodal, consisting of both text and visual components. For simplicity, we do not distinguish between system prompts and user instructions in text input. Let $\mathbf{x}^t = \{x_1, x_2, \dots, x_M\}$ denote the token sequence encoded by the text encoder, representing a textual feature sequence of length M . Similarly, let $\mathbf{x}^v = \{x_{M+1}, x_{M+2}, \dots, x_{M+N}\}$ represent the visual token sequence encoded by the vision encoder, with length N . These sequences are concatenated into a unified input sequence $\mathbf{x} = \{x_1, x_2, \dots, x_{M+N}\}$ before being fed into the LVLM.

The LVLM processes this input token sequence \mathbf{x} through L Transformer layers. The output at layer $l + 1$, denoted as $\mathbf{h}^{(l+1)}$, is computed using multi-head self-attention [31]:

$$\mathbf{h}^{(l+1)} = \mathbf{h}^{(l)} + \sum_{n=1}^{N_h} \mathcal{A}_n^l(\mathbf{h}^{(l)}) \mathbf{P}_n^l \quad (1)$$

where N_h is the total number of heads in a Transformer layer, d is the dimension of the operation space of each head; $\mathcal{A}_n^l(\cdot)$ is the attention operator of the n -th head in the l -th layer; $\mathbf{P}_n^l \in \mathbb{R}^{d \times dN_h}$ maps the activated output of attention head back to the operation space of the l -th Transformer layer. Each layer performs self-attention to capture interactions between text and visual features. At the final layer (layer L), the hidden states $\mathbf{h}^{(L)}$ are passed through an affine layer to produce logits of size equal to the vocabulary, followed by Softmax normalization to generate the probability distribution for the next token y_t :

$$p(y_t | y_{<t}) = \text{Softmax}(\text{Affine}(\mathbf{h}_t^{(L)}))$$

where $y_{<t}$ represents the previously generated tokens.

3.2. Modeling Trusted and Hallucinated Manifolds of Attention Activations

Our method, Scalpel, is based on two key findings from studies on LLMs and LVLMs. First, these models often know the correct answer but fail to express it clearly [12, 24, 32]. Second, their activation space has key directions that guide truthful responses [4, 26]. Earlier methods like ITI [16] and ICT [6] reduce hallucinations by steering attention heads toward trusted activation spaces. Yet, they

use fixed correction directions for all activations in a head, which may not be ideal. Scalpel improves this by customizing intervention directions for different activations during inference, even within the same attention head. To do this efficiently, we separately discretize and tokenize trusted and hallucinated manifolds, then create a one-to-one mapping between them. GMMs [1] are well-suited for this task. We use GMMs to model attention activations from both trusted and hallucinated data, approximating their manifolds.

Trusted activation manifolds are built from valid (image, \mathbf{Q}, \mathbf{A}) triplets (e.g., \mathbf{Q} : What is in the image? \mathbf{A} : Zebra.), extracting attention activations across all layers/heads, as shown in the left part of Figure 1. Hallucinated manifolds are created by perturbing images while keeping QA pairs correct, or by altering specific image regions (e.g., zebra bounding boxes). For each attention head/layer, we extract three manifolds: (1) trusted, (2) image-perturbed hallucinated, (3) object-perturbed hallucinated. Activation distributions differ slightly between image and object levels, leading to different intervention directions. At the object level, as shown in Figure 2, most background remains unchanged, so only specific components need large-scale intervention. However, intervention principles are identical, so we omit level distinctions in the following. Our goal is to map hallucinated to trusted manifolds, enabling corrective adjustments to activations. Let ρ_H denote the hallucinated manifold's distribution with sample \mathbf{z}_0 , and ρ_T the trusted with \mathbf{z}_1 . The optimal mapping is given by the entropic optimal transport (EOT) problem [22]:

$$\min_{\pi \in \Pi(\rho_H, \rho_T)} \int \|\mathbf{z}_0 - \mathbf{z}_1\|^2 d\pi - \epsilon h(\pi) \quad (2)$$

where $\pi(\mathbf{z}_0, \mathbf{z}_1)$ is the transport plan (coupling), $\Pi(\rho_H, \rho_T)$ the joint distributions with these marginals, and h the differential entropy:

$$h(\rho) \triangleq - \int \rho(\mathbf{z}) \log \rho(\mathbf{z}) d\mathbf{z}. \quad (3)$$

Directly solving the EOT problem (Eq. 2) from hallucinatory to trusted activations is difficult. Leonard reformulates it as an equivalent Schrödinger bridge problem (SBP) for tractability [15]:

$$\min_{\mathbf{u} \in \mathcal{U}} \mathbb{E}_{t \sim \rho_t} \left[\int_0^1 \frac{1}{2\epsilon} \|\mathbf{u}_t(\mathbf{z}_t)\|^2 dt \right], \quad (4)$$

$$d\mathbf{z}_t = \mathbf{u}_t(\mathbf{z}_t) dt + \sqrt{\epsilon} d\mathbf{w}_t, \quad (5)$$

$$\mathbf{z}_0 \sim \rho_H, \quad \mathbf{z}_1 \sim \rho_T, \quad (6)$$

where \mathcal{U} is the set of adapted finite-energy controls (i.e., drift in diffusion/SDEs). The goal is minimal-energy control ensuring initial distribution ρ_H and terminal ρ_T . We solve this SBP to derive the optimal path from hallucination to trusted manifolds.

3.3. Optimal Transport Mapping Between Trusted and Hallucinated GMMs

Both trusted/hallucinated GMMs contain multiple components. When an activation belongs to a hallucinated component, mapping requires not only identifying its trusted counterpart but determining the optimal transformation path. To address this, we propose an alignment algorithm superior to random matching. Intuitively, minimal corrections preserve data manifold integrity, thus we seek minimum-cost flow mapping between components, as depicted in the right part of Figure 1.

This process is performed independently per attention head. Let hallucinated GMM (for a head) be:

$$\mathbf{z}_0 \sim \rho_H \approx \sum_{i=1}^{N_0} w_0^i \mathcal{N}(\mu_0^i, \Sigma_0^i), \quad (7)$$

and trusted GMM:

$$\mathbf{z}_1 \sim \rho_T \approx \sum_{j=1}^{N_1} w_1^j \mathcal{N}(\mu_1^j, \Sigma_1^j), \quad (8)$$

where μ_0^i, Σ_0^i and μ_1^j, Σ_1^j are mean/covariance parameters $\forall i, j$. $\mathbf{z}_0, \mathbf{z}_1$ represent hallucinated/trusted activations.

Eq. (4) becomes optimal mapping between GMMs:

$$\min_{\mathbf{u} \in \mathcal{U}} \mathbb{E} \left[\int_0^1 \|\mathbf{u}_t(\mathbf{z})\|^2 dt \right], \quad d\mathbf{z} = \mathbf{u}_t(\mathbf{z}) dt + \sqrt{\epsilon} d\mathbf{w} \quad (9)$$

with $\mathbf{z}_0, \mathbf{z}_1$ satisfying Eq. (7) and (8).

This formulation physically avoids excessive perturbation of LVLM attention activations, preserving visual-language alignment. Instead, it achieves hallucinated-to-trusted state shifts via minimal integral intervention.

The Schrödinger bridge solves optimal transport between distributions. Bunne et al. [3] derived a closed-form Gaussian bridge solution for single Gaussians (i.e., $N_0 = N_1 = 1$ in Eq. 9 constrained by Eq. 7,8). This yields the most probable diffusion path under Brownian motion, with Gaussian marginals at all times. Rapakoulias et al. [23] extended this to GMMs by combining Gaussian bridges via linear programming, ensuring theoretical feasibility and performance bounds.

Thus, we establish optimal hallucination-to-trust GMM mapping (Proposition 1), maximally preserving LVLM vision-language alignment.

Proposition 3.1. *(Optimal GMM bridge policy for hallucination-to-trust transition) For the GMM bridge problem in Eq. (9), let $\mathbf{u}_{t|ij}$ be the optimal control policy for the Gaussian bridge between hallucinated component i ($\mathcal{N}(\mu_0^i, \Sigma_0^i)$) and trusted component j ($\mathcal{N}(\mu_1^j, \Sigma_1^j)$), with induced flow $\rho_{t|ij}$ and optimal cost J_{ij} .*

Consider this linear program:

$$\min_{\lambda} \sum_{i,j} \lambda_{ij} J_{ij}$$

under optimal transport constraints with $\lambda_{ij} \geq 0, \forall i, j$:

$$\begin{aligned} \sum_{j=1}^{N_1} \lambda_{ij} &= w_0^i, & i &= 1, \dots, N_0, \\ \sum_{i=1}^{N_0} \lambda_{ij} &= w_1^j, & j &= 1, \dots, N_1. \end{aligned}$$

The solution λ_{ij}^* gives the optimal lower bound for Eq. (9). The optimal mixture policy:

$$\mathbf{u}_t(\mathbf{z}) = \sum_{i,j} \mathbf{u}_{t|ij}(\mathbf{z}) \frac{\rho_{t|ij}(\mathbf{z}) \lambda_{ij}^*}{\sum_{r,\ell} \rho_{t|r\ell}(\mathbf{z}) \lambda_{r\ell}^*}, \quad (10)$$

is feasible for (9) with induced flow:

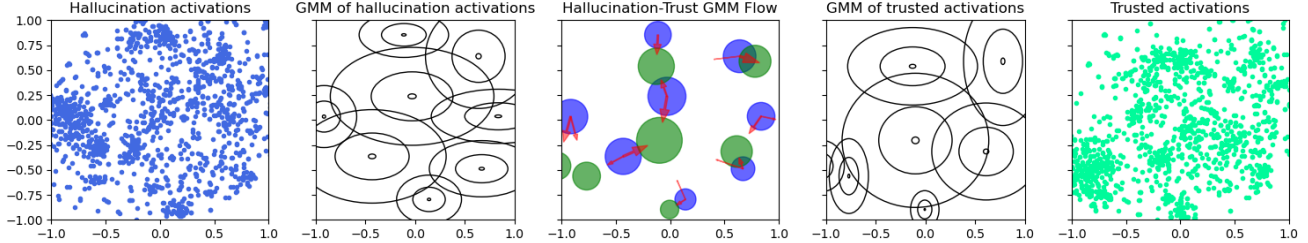
$$\rho_t(\mathbf{z}) = \sum_{i,j} \rho_{t|ij}(\mathbf{z}) \lambda_{ij}^*.$$

Proof sketch. For system $d\mathbf{z}_t = \mathbf{u}(\mathbf{z}_t) dt + \sqrt{\epsilon} d\mathbf{w}_t$, the Fokker–Planck–Kolmogorov (FPK) [13] equation uniquely determines ρ_t 's evolution and enables control policy derivation. The parabolic PDE guarantees existence/uniqueness of ρ_t , forming the basis for state-feedback control minimizing quadratic costs. Additive Gaussian noise and linear dynamics ensure tractability via Riccati equations, yielding closed-form optimal policies. \square

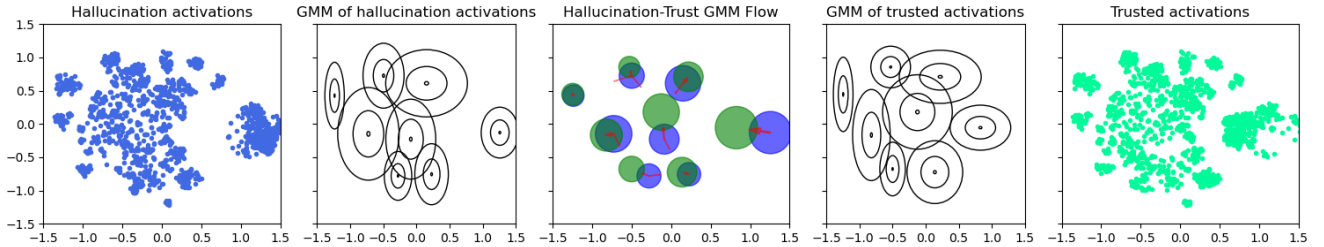
Per Proposition 3.1, the solution uses a mixture strategy weighting conditional policies by $\lambda_{ij}^* \rho_{t|ij}(\mathbf{z})$, normalized by $\sum_{i,j} \rho_{t|ij}(\mathbf{z}) \lambda_{ij}^*$. Since $\rho_{t|ij}(\mathbf{z})$ is Gaussian centered at the (i, j) -bridge mean at t , this prioritizes strategies with means closer to \mathbf{z} . Applied independently per attention head, the Schrödinger bridge framework maps hallucinated to trusted Gaussian components with minimal cost. Here λ_{ij}^* represents transport weight from hallucinated i to trusted j . For each i , select $j^* = \arg \max_j \lambda_{ij}^*$ as the trusted counterpart for mitigation (used next section). Figure 2 shows optimal transfer examples from hallucination to trusted manifold. These cases, from different attention heads, demonstrate both image-level and object-level interventions. We observe that tailored interventions can be applied for distinct tokens, enabling greater customization.

3.4. Hallucination Mitigation Based on Optimal Mapping Between Manifolds

To identify critical attention heads, we train logistic regression probes over all L layers and N_h heads of the vision-language transformer. Given activation tensors $\mathcal{A} \in$



(a) This comparison shows the distribution of trusted and hallucinated attention activations at the image level. The activations are extracted from the 73rd attention head in layer 1 of LLaVA-1.5. As seen in the middle image, most of the eight hallucination components require noticeable interventions, varying in both direction and scale.



(b) This comparison shows distributions of trusted and hallucinated object-level attention activations, illustrating GMM transitions. Activations originate from LLaVA-1.5's 12th layer, 62nd head. Of 8 hallucinated components, 6-7 require minimal intervention while the rightmost needs substantial correction. This occurs because hallucinations typically affect single bounding boxes, leaving other image areas intact - as shown in Figure 1 (zebra example).

Figure 2. Comparison of the distributions of trusted and hallucinated attention activations at the image and object levels, including the component composition of GMMs and the transition flow from the hallucinated GMMs to the trusted GMMs. For simplicity, we use t-SNE [30] to map the original attention activations into a two-dimensional space before performing all subsequent operations.

$\mathbb{R}^{B \times L \times N_h \times d}$ (batch size B , dimension d), we train a logistic model on each head's activations to distinguish hallucinated (1) vs factual (0) inputs using cross-entropy loss with L_2 -regularized weights. The accuracy matrix $\mathcal{M} \in \mathbb{R}^{L \times N_h}$ reveals top- k heads for intervention analysis (Figure 1), where dark orange highlights indicate strong hallucination discrimination capacity.

The mitigation strategy dynamically adjusts key attention heads during answer generation to influence outputs. At each step, we extract the current token's high-dimensional attention vector, reflecting the model's internal state critical for next-word prediction in autoregressive models. Using pre-trained hallucinated and trusted GMMs (with multiple components), and their optimal mapping (Section 3.3), we analyze activation distributions to determine most probable component membership. This clustering interprets activation roles by comparing positions against learned patterns. Let $\mathbf{z}_{\text{current}} = \mathbf{z}_t^{(l,h)} \in \mathbb{R}^d$ denote the output activation vector at step t from layer l , head h . Compute posterior probabilities for hallucination GMM components:

$$\mathcal{P}(r|\mathbf{z}) = \frac{w_0^r \mathcal{N}(\mathbf{z}|\mu_0^r, \Sigma_0^r)}{\sum_{i=1}^{N_h} w_0^i \mathcal{N}(\mathbf{z}|\mu_0^i, \Sigma_0^i)}. \quad (11)$$

Let

$$r^* = \arg \max_r \mathcal{P}(r | \mathbf{z}_{\text{current}}) \quad (12)$$

denote the hallucinated Gaussian component to which the current activation $\mathbf{z}_{\text{current}}$ is most likely assigned, and let

$$c = \max_r \mathcal{P}(r | \mathbf{z}_{\text{current}}) \quad (13)$$

represent the corresponding assignment probability.

The intervention uses precomputed Schrödinger bridge mappings (Section 3.3). When identifying a hallucinated component via Eq. (12), we retrieve its trusted counterpart through λ_{ij}^* in Eq. (10) and compute the transfer vector as $\mathbf{v}_{r^*} = \mu_1^{j^*} - \mu_0^{r^*}$, where $j^* = \arg \max_j \lambda_{r^*j}$.

Intervention strength combines base coefficient α_{base} and Eq. (13) confidence:

$$\alpha_{\text{dynamic}} = \alpha_{\text{base}} \cdot c \quad (14)$$

Strong matches ($c \approx 1$) get stronger interventions, while ambiguous cases receive milder adjustments to maintain stability. Apply the scaled vector:

$$\mathbf{h}^{(l+1)} = \mathbf{h}^{(l)} + \sum_{n=1}^{N_h} \left[\mathcal{A}_n^l(\mathbf{h}^{(l)}) + \mathbf{1}_{\text{top-}k}(l, n) \alpha_{\text{dynamic}} \mathbf{v}_{r^*} \right] \mathbf{P}_n^l \quad (15)$$

Only top- k heads (Figure 1) get modified via indicator function $\mathbf{1}_{\text{top-}k}$, ensuring minimal perturbation while guiding activations toward trusted distributions. This correction applies at each generation step to reduce hallucinations while preserving generation coherence.

Table 1. Performance comparison of Scalpel and other baseline methods on the POPE benchmark across three datasets — MSCOCO, A-OKVQA, and GQA — using the LLaVA-1.5-7B model. **Bold** values indicate the best performance on each dataset and metric.

Acc.↑/F1↑	MS COCO			A-OKVQA			GQA		
	Random	Popular	Adversarial	Random	Popular	Adversarial	Random	Popular	Adversarial
Vanilla [19]	83.29/81.33	81.88/80.06	78.96/77.57	83.45/82.56	79.90/79.59	74.04/75.15	83.73/82.95	78.17/78.37	75.08/76.06
VCD [14]	87.73/87.16	85.38/85.06	80.88/81.3	86.15/86.34	81.85/82.82	74.97/77.73	86.65/86.99	80.73/82.24	76.09/78.78
OPERA [10]	89.20/88.81	86.64/86.62	81.24/81.38	88.02/84.59	83.22/84.67	73.82/77.91	88.13/88.91	79.27/82.11	75.00/78.71
ICT [6]	89.1/88.48	86.76/86.40	83.83/83.84	89.3/89.40	83.4/84.45	75.56/78.68	89.3/89.49	80.86/82.64	77.4/80.11
Scalpel (ours)	90.67/90.74	87.87/88.36	85.97/86.00	89.87/89.93	85.00/85.18	78.40/79.71	89.93/89.87	84.57/85.31	81.00/82.09

4. Experiments

4.1. Benchmarks and Experimental Setup

Polling-based Object Probing Evaluation (POPE). POPE [17] evaluates object hallucinations in LVLMs via binary queries (e.g., “Is there a chair?”). Unlike caption-based methods, it directly probes object recognition and hallucination. The balanced dataset (27K pairs) contains 50% real/50% absent objects from COCO [18], A-OKVQA [25], and GQA [11]. Three sampling strategies: random, popular (frequent objects), adversarial (challenging cases). Evaluation uses Accuracy and F1.

Multimodal Model Evaluation (MME). MME [9] comprehensively assesses LVLMs across 14 subtasks: 10 perception, 4 cognition. Perception includes object existence/count (object hallucinations), position/color (attribute hallucinations). Cognition covers commonsense reasoning (CSR), numerical, translation, and code reasoning. Accuracy-based metrics used.

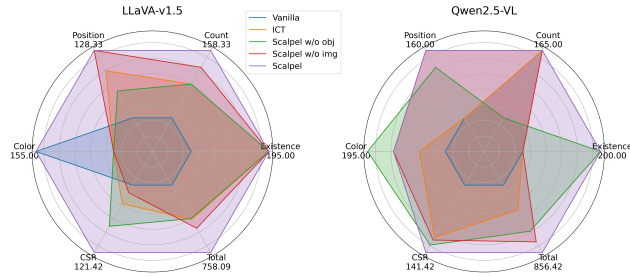


Figure 3. On the MME benchmark, Scalpel outperforms prior SOTA methods - ICT, Vanilla LLaVA-1.5 and Qwen2.5-VL. The radar chart highlights improvements across key categories: existence, location, counting, color perception, common sense reasoning, and overall performance.

Implementation details. We evaluated Scalpel on two established LVLMs: LLaVA-1.5-7B [19] and Qwen2.5-VL-7B [2], comparing with VCD [19], OPERA, and ICT¹ hallucination mitigation methods. Hyperparameters included: top- k head selection (Eq. (15)), intervention strength α_{base} (Eq. (14)), and GMM component count N_0 (Eq. (7)). To simplify tuning while preserving discriminative power, we enforced equal component counts for trusted/hallucinated

GMMs. For head selection, we adopted ICT’s framework [6] with 1,500 trusted vs. hallucination samples (image/object-level), training logistic regression classifiers on attention head activations to identify top- k critical heads. This prioritized heads showing significant activation patterns during hallucinatory phases.

4.2. Results and Discussion

Tables 1, 2, and 3 compare Scalpel with leading methods—VCD, OPERA, and ICT—across nine POPE datasets under LLaVA-1.5 and Qwen2.5-VL frameworks. Scalpel excels on MS COCO, A-OKVQA, and GQA, outperforming prior methods in Random, Popular, and Adversarial subsets. Compared to Vanilla, it improves accuracy by 7.61% and F1 by 8.88%, with notable gains in adversarial cases (e.g., +10.87% F1 on MS COCO-Adversarial), demonstrating strong robustness and generalization. Against ICT—the previous best—it achieves average relative improvements of 2.43% (Acc.) and 1.81% (F1), with no performance drop. Largest gains appear in Popular and Adversarial subsets (e.g., +4.59% Acc. on GQA-Popular), highlighting its ability to reduce bias and handle hard data.

Table 2 presents detailed analysis of Scalpel’s modular intervention vs. ICT under LLaVA. Image-Level (w/o obj) gains 1.63% avg F1 (+4.93% peak on A-OKVQA-Random), with strong adversarial performance (+2.47% Acc. on COCO-Adversarial). Object-Level (w/o img) improves 1.85% avg F1 (+5.85% peak) while avoiding ICT’s 84.06 → 84.47 Acc. drop on GQA-Popular. Combined, Scalpel achieves max gains (+2.43% Acc./1.81% F1) with super-additive effects: joint modules deliver +8.22% F1 on COCO-Adversarial over ICT’s single module. Crucially, all 18 comparative indicators (9 subsets × Acc/F1) show strict dominance, validating Scalpel’s hierarchical design through both superior individual modules and synergistic collaboration.

Table 3 confirms Scalpel’s advantages in Qwen2.5-VL with +5.19% average Acc. (peak +9.94% on COCO-Random) and +7.16% F1 improvement (peak +9.20% COCO-Popular), achieving 85.40 F1 on GQA-Adversarial

¹All ICT results are from our re-implementation (based on <https://github.com/THU-BPM/ICT>) for fair comparison.

Table 2. Performance comparison of Scalpel and the previous SOTA method ICT using the LLaVA-1.5-7B model on the POPE benchmark across three datasets: MS COCO, A-OKVQA, and GQA. Results are shown for three configurations: image-level intervention (w/o obj), object-level intervention (w/o img), and their combination. The outputs marked with a blue background represent the results of our Scalpel.

Acc.↑/F1↑	COCO			A-OKVQA			GQA		
	Random	Popular	Adversarial	Random	Popular	Adversarial	Random	Popular	Adversarial
Vanilla [19]	83.29/81.33	81.88/80.06	78.96/77.57	83.45/82.56	79.90/79.59	74.04/75.15	83.73/82.95	78.17/78.37	75.08/76.06
ICT w/o obj	87.53/86.20	86.56/85.31	85.1/83.97	85.33/85.16	88.7/88.16	78.7/79.81	89.06/88.53	84.73/84.69	81.43/81.97
Scalpel w/o obj	89.07/88.18	87.07/86.24	85.77/85.29	89.53/89.36	85.50/85.29	79.30/79.90	89.67/89.40	84.63/84.70	81.47/82.08
ICT w/o img	89.4/88.85	86.83/86.49	83.7/83.82	83.23/84.34	89.13/89.26	75.6/78.72	89.2/89.40	84.06/83.44	74.3/74.91
Scalpel w/o img	89.90/90.08	87.6/86.97	85.53/84.66	89.47/89.27	85.27/85.22	78.47/80.18	89.87/89.81	84.47/85.04	80.93/81.89
ICT [6]	89.1/88.48	86.76/86.40	83.83/83.84	89.3/89.40	83.4/84.45	75.56/78.68	89.3/89.49	80.86/82.64	77.4/80.11
Scalpel (ours)	90.67/90.74	87.87/88.36	85.97/86.00	89.87/89.93	85.00/85.18	78.40/79.71	89.93/89.87	84.57/85.31	81.00/82.09

Table 3. Performance comparison of Scalpel and the previous SOTA method ICT using the Qwen2.5-VL-7B model on the POPE benchmark across three datasets: MS COCO, A-OKVQA, and GQA. Results are shown for three configurations: image-level intervention (w/o obj), object-level intervention (w/o img), and their combination. The results highlighted with a blue background were produced by our Scalpel.

Acc.↑/F1↑	COCO			A-OKVQA			GQA		
	Random	Popular	Adversarial	Random	Popular	Adversarial	Random	Popular	Adversarial
Vanilla [2]	85.4/82.97	85.13/82.71	84.83/82.42	87.76/86.41	86.43/85.15	81.5/80.78	87.1/85.63	84/82.74	81.6/80.65
ICT w/o obj	86.4/84.31	86.3/84.27	85.7/83.53	89.93/89.15	87.46/86.76	82.5/82.54	88.06/87.01	83.9/83.23	81.63/81.17
Scalpel w/o obj	86.27/84.84	88.97/87.87	86.57/84.87	91.20/90.54	88.83/88.37	81.70/80.94	88.03/89.67	84.43/84.16	85.47/85.96
ICT w/o img	85.4/82.97	85.4/83.07	85.2/82.90	88.76/87.64	86.63/85.50	81.7/81.16	87.16/85.66	83.93/82.67	81.33/80.40
Scalpel w/o img	86.37/84.26	85.80/83.60	85.37/82.98	88.73/87.66	87.17/85.99	82.57/82.08	87.73/86.02	85.27/85.89	83.00/82.29
ICT [6]	87.53/85.84	86.76/84.94	86.16/84.32	88.96/87.90	87.43/86.39	83.6/83.02	88.96/87.89	86.43/85.47	84.1/83.53
Scalpel (ours)	91.17/90.41	90.80/90.33	88.83/88.49	91.00/90.55	90.50/90.41	84.97/85.82	89.20/89.84	87.20/86.68	85.90/85.40

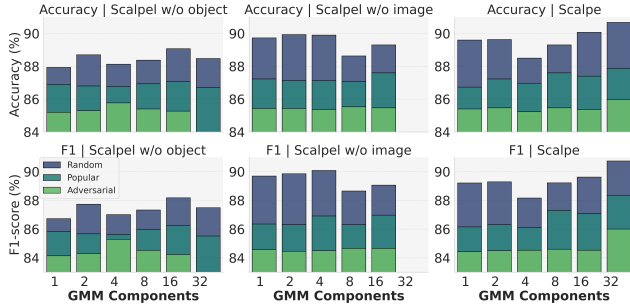


Figure 4. Ablation study of Scalpel under different GMM component settings, evaluated on the POPE benchmark (MS COCO dataset) with LLaVA-1.5-7B.

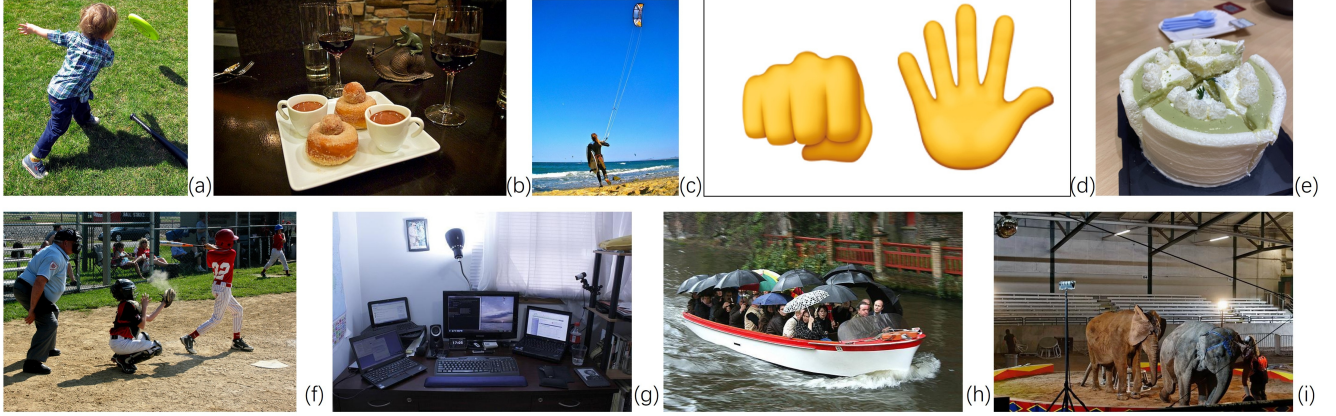
(vs. 80.65). Modular analysis shows Image-Level (w/o obj) +3.07% avg F1 (A-OKVQA-Random 90.54 vs. 89.15) and Object-Level (w/o img) +1.92% avg F1 (GQA-Popular 85.89 vs. 82.67). Dual-module synergy delivers 1.67× F1 gain over ICT (Scalpel 2.97% vs. ICT 1.78%), maintaining 1.77% absolute advantage on GQA-Adversarial. Adversarial F1 gains exceed ICT by 1.65× (GQA: 5.89% vs. 3.57%).

Figure 3 shows multi-dimensional improvements: LLaVA-based Scalpel scores 758.09 (+8.52% vs. Vanilla), excelling in counting (+14.46%), positioning (+14.93%), and common sense (+11.84%). Removing modules reduces performance (w/o obj: 728.09/+4.23%; w/o

img: 736.66/+5.45%), highlighting image-object synergy. Qwen-based Scalpel scores 851.42 (+6.14%), achieving SOTA in positioning (+14.29%), color (+5.56%), and common sense (+15.80%). Module analysis reveals: image removal maintains positional/color performance but degrades reasoning (+12.86% vs. +15.80%), while object removal causes 9.09% counting drop but improves color (+8.33%) and reasoning (+14.03%) via reduced interference. Scalpel surpasses ICT (822.14/+2.49%), with absolute dominance in complex reasoning (141.42 vs. 137.85).

4.3. Ablation study

Scalpel's efficacy was validated through three aspects: GMM components (intervention granularity), image-level, and object-level interventions. Tables 2, 3, and Figure 4 present ablation studies. Specifically, Tables 2 and 3 compare Scalpel variants (LLaVA-1.5/Qwen2.5-VL) across 9 POPE subsets when removing modules. Quantitative results show: adding image-level intervention improves LLaVA by +7.46% Acc./+8.43% F1 (Qwen: +2.32%/+3.69%); object-level adds +7.37% Acc./+8.14% F1 (LLaVA) and +1.09%/+1.52% (Qwen). Combined modules show peak gains: +7.61% Acc./+8.78% F1 (LLaVA) and +4.70% Acc./+6.48% F1 (Qwen). These cross-model improvements validate dual levels' critical role in hallucination mitigation.



(a) Q: Is there a frisbee in the image? **GT**: Yes. **Qwen2.5-VL**: No. **ICT**: No. **Scalpel**: Yes.
 (b) Q: Is there a floor in the image? **GT**: No. **Qwen2.5-VL**: Yes. **ICT**: Yes, there is a floor in the image. **Scalpel**: No.
 (c) Q: Is the person under the kite? **GT**: Yes. **Qwen2.5-VL**: No. **ICT**: No. **Scalpel**: Yes.
 (d) Q: May I ask if in the game of finger-guessing game, did the right side of the picture win? **GT**: Yes. **Qwen2.5-VL**: No. **ICT**: No. **Scalpel**: Yes.
 (e) Q: Here is a picture of the cake I cut. Did I cut it at least twice? **GT**: Yes. **Qwen2.5-VL**: no, you did not cut the cake in half twice. the image shows a single-layer cake that has been partially sliced, but likely once, to reveal it's the inside. however, the top of the cake remains intact and the sides are still smooth and uncut. **ICT**: no, you did not cut the cake in half twice. the image shows a single-layer cake that has been partially sliced. **Scalpel**: Yes.
 (f) Q: Is there a chair in the image? **GT**: Yes. **Qwen2.5-VL**: No. **ICT**: No. **Scalpel**: Yes.
 (g) Q: Is the light under the computer in the image? **GT**: No. **Qwen2.5-VL**: Yes. **ICT**: Yes. **Scalpel**: No.
 (h) Q: Is the blue umbrella under the black umbrella? **GT**: Yes. **Qwen2.5-VL**: No. **ICT**: No. **Scalpel**: Yes.
 (i) Q: Is the brown elephant in front of the gray elephant? **GT**: No. **Qwen2.5-VL**: Yes. **ICT**: Yes. **Scalpel**: No.

Figure 5. A comparative analysis of Scalpel, ICT, and the original Qwen2.5-VL-7B across selected test cases is presented. **Q** denotes the question, **GT** represents the ground truth, and each method’s answer follows its name in **bold**. Extended **hallucinated responses** are highlighted in **red** for emphasis. Notably, the original questions included the instruction “Please answer yes or no” immediately after the question mark, which has been omitted to optimize space usage.

Figure 4 analyzes GMM component count’s impact on hallucination reduction and accuracy. Tests on COCO’s POPE subsets (Random, Popular, Adversarial) evaluated 1–32 components. Higher counts improve performance, with 32 components yielding best results across all subsets. Image-level intervention peaks at 16 components for Random/Popular, fewer for Adversarial. Object-level requires higher counts even in adversarial cases. Complementary patterns justify recommending full Scalpel with 32 GMM components, balancing granularity needs across intervention levels and data complexities.

Figure 5 presents qualitative comparisons. Scalpel surpasses ICT in object perception, spatial analysis, scenario suitability, and action trace recognition. First, compared to ICT/Vanilla Qwen2.5-VL, Scalpel enhances image understanding accuracy by removing hallucinated elements (e.g., non-visible floors) and detecting missed objects (e.g., frisbees/chairs), significantly reducing hallucinations. Second, Scalpel perfectly matches GT in object positioning (e.g., occlusion under kites/umbrellas) and spatial arrangements (elephant positioning), while ICT errors arise from over-reliance on localized features/color cues. Third, Scalpel detects subtle visual traces (e.g., cake cuts) rather than surface appearances. It also eliminates ICT’s redundant as-

sumptions/logical inconsistencies (e.g., “requires verification”), producing streamlined reasoning paths. These advantages reflect superior vision-language alignment and noise filtering during complex reasoning.

5. Conclusion

To correct hallucinated attention activations in LVLM Transformers without added computational cost, we propose Scalpel. This method models hallucinated and trusted attention activations via Gaussian Mixture Models (GMMs), yielding hallucinated and trusted GMMs respectively. The Schrödinger Bridge (equivalent to entropic optimal transport) then constructs the minimal transport-cost correction scheme by treating these GMMs as marginal distributions. This preserves LVLMs’ data-driven learning capabilities while effectively suppressing hallucinations. Experiments across datasets show Scalpel achieves SOTA performance, surpassing non-customized methods. A promising future direction is investigating refined correction formulations via the infinite-component limit of GMMs.

References

[1] Robust text-independent speaker identification using gaussian mixture speaker models. *IEEE transactions on speech*

and audio processing, 3(1):72–83, 1995. 3

[2] Shuai Bai, Keqin Chen, Xuejing Liu, Jialin Wang, Wenbin Ge, Sibo Song, Kai Dang, Peng Wang, Shijie Wang, Jun Tang, et al. Qwen2. 5-vl technical report. *arXiv preprint arXiv:2502.13923*, 2025. 2, 6, 7

[3] Charlotte Bunne, Ya-Ping Hsieh, Marco Cuturi, and Andreas Krause. The schrödinger bridge between gaussian measures has a closed form. In *International Conference on Artificial Intelligence and Statistics*, pages 5802–5833. PMLR, 2023. 4

[4] Collin Burns, Haotian Ye, Dan Klein, and Jacob Steinhardt. Discovering latent knowledge in language models without supervision. *arXiv preprint arXiv:2212.03827*, 2022. 3

[5] Cong Chen, Mingyu Liu, Chenchen Jing, Yizhou Zhou, Fengyun Rao, Hao Chen, Bo Zhang, and Chunhua Shen. Perturbolla: Reducing multimodal hallucinations with perturbative visual training. *arXiv preprint arXiv:2503.06486*, 2025. 1, 2

[6] Junzhe Chen, Tianshu Zhang, Shiyu Huang, Yuwei Niu, Linfeng Zhang, Lijie Wen, and Xuming Hu. Ict: Image-object cross-level trusted intervention for mitigating object hallucination in large vision-language models. *Proceedings of the IEEE/CVF Conference on Computer Vision and Pattern Recognition*, 2025. 2, 3, 6, 7

[7] Wei-Lin Chiang, Zhuohan Li, Ziqing Lin, Ying Sheng, Zhanghao Wu, Hao Zhang, Lianmin Zheng, Siyuan Zhuang, Yonghao Zhuang, Joseph E Gonzalez, et al. Vicuna: An open-source chatbot impressing gpt-4 with 90%* chatgpt quality. *See <https://vicuna.lmsys.org> (accessed 14 April 2023)*, 2(3):6, 2023. 2

[8] Alessandro Favero, Luca Zancato, Matthew Trager, Siddharth Choudhary, Pramuditha Perera, Alessandro Achille, Ashwin Swaminathan, and Stefano Soatto. Multi-modal hallucination control by visual information grounding. In *Proceedings of the IEEE/CVF Conference on Computer Vision and Pattern Recognition*, pages 14303–14312, 2024. 1, 2

[9] Chaoyou Fu, Peixian Chen, Yunhang Shen, Yulei Qin, Mengdan Zhang, Xu Lin, Jinrui Yang, Xiawu Zheng, Ke Li, Xing Sun, et al. Mme: A comprehensive evaluation benchmark for multimodal large language models. *arXiv preprint arXiv:2306.13394*, 2023. 2, 6

[10] Qidong Huang, Xiaoyi Dong, Pan Zhang, Bin Wang, Conghui He, Jiaqi Wang, Dahua Lin, Weiming Zhang, and Nenghai Yu. Opera: Alleviating hallucination in multi-modal large language models via over-trust penalty and retrospection-allocation. In *Proceedings of the IEEE/CVF Conference on Computer Vision and Pattern Recognition*, pages 13418–13427, 2024. 1, 2, 6

[11] Drew A Hudson and Christopher D Manning. Gqa: A new dataset for real-world visual reasoning and compositional question answering. In *Proceedings of the IEEE/CVF conference on computer vision and pattern recognition*, pages 6700–6709, 2019. 6

[12] Saurav Kadavath, Tom Conerly, Amanda Askell, Tom Henighan, Dawn Drain, Ethan Perez, Nicholas Schiefer, Zac Hatfield-Dodds, Nova DasSarma, Eli Tran-Johnson, et al. Language models (mostly) know what they know. *arXiv preprint arXiv:2207.05221*, 2022. 3

[13] A Kolmogorov. Über die analytischen methoden in der wahrscheinlichkeitstheorie. *Math Annal*, 104:415–458, 1931. 4

[14] Sicong Leng, Hang Zhang, Guanzheng Chen, Xin Li, Shijian Lu, Chunyan Miao, and Lidong Bing. Mitigating object hallucinations in large vision-language models through visual contrastive decoding. In *Proceedings of the IEEE/CVF Conference on Computer Vision and Pattern Recognition*, pages 13872–13882, 2024. 1, 2, 6

[15] Christian Léonard. A survey of the schrödinger problem and some of its connections with optimal transport. *Discrete and Continuous Dynamical Systems-Series A*, 34(4):1533–1574, 2014. 3

[16] Kenneth Li, Oam Patel, Fernanda Viégas, Hanspeter Pfister, and Martin Wattenberg. Inference-time intervention: Eliciting truthful answers from a language model. *Advances in Neural Information Processing Systems*, 36:41451–41530, 2023. 2, 3

[17] Yifan Li, Yifan Du, Kun Zhou, Jinpeng Wang, Wayne Xin Zhao, and Ji-Rong Wen. Evaluating object hallucination in large vision-language models. *arXiv preprint arXiv:2305.10355*, 2023. 2, 6

[18] Tsung-Yi Lin, Michael Maire, Serge Belongie, James Hays, Pietro Perona, Deva Ramanan, Piotr Dollár, and C Lawrence Zitnick. Microsoft coco: Common objects in context. In *Computer vision–ECCV 2014: 13th European conference, zurich, Switzerland, September 6–12, 2014, proceedings, part v 13*, pages 740–755. Springer, 2014. 6

[19] Haotian Liu, Chunyan Li, Qingyang Wu, and Yong Jae Lee. Visual instruction tuning. *Advances in neural information processing systems*, 36:34892–34916, 2023. 1, 2, 6, 7

[20] Ziyu Liu, Yuhang Zang, Xiaoyi Dong, Pan Zhang, Yuhang Cao, Haodong Duan, Conghui He, Yuanjun Xiong, Dahua Lin, and Jiaqi Wang. Mia-dpo: Multi-image augmented direct preference optimization for large vision-language models. *arXiv preprint arXiv:2410.17637*, 2024. 1, 2

[21] Jinda Lu, Junkang Wu, Jinghan Li, Xiaojun Jia, Shuo Wang, YiFan Zhang, Junfeng Fang, Xiang Wang, and Xiangnan He. Dama: Data-and model-aware alignment of multi-modal llms. *arXiv preprint arXiv:2502.01943*, 2025. 1, 2

[22] Gabriel Peyré, Marco Cuturi, et al. Computational optimal transport: With applications to data science. *Foundations and Trends® in Machine Learning*, 11(5-6):355–607, 2019. 3

[23] George Rapakoulias, Ali Reza Pedram, and Panagiotis Tsiotras. Go with the flow: Fast diffusion for gaussian mixture models. *arXiv preprint arXiv:2412.09059*, 2024. 4

[24] William Saunders, Catherine Yeh, Jeff Wu, Steven Bills, Long Ouyang, Jonathan Ward, and Jan Leike. Self-critiquing models for assisting human evaluators. *arXiv preprint arXiv:2206.05802*, 2022. 3

[25] Dustin Schwenk, Apoorv Khandelwal, Christopher Clark, Kenneth Marino, and Roozbeh Mottaghi. A-okvqa: A benchmark for visual question answering using world knowledge. In *European conference on computer vision*, pages 146–162. Springer, 2022. 6

[26] Nishant Subramani, Nivedita Suresh, and Matthew E Peters. Extracting latent steering vectors from pretrained language models. *arXiv preprint arXiv:2205.05124*, 2022. 3

[27] Zhiqing Sun, Sheng Shen, Shengcao Cao, Haotian Liu, Chunyuan Li, Yikang Shen, Chuang Gan, Liang-Yan Gui, Yu-Xiong Wang, Yiming Yang, et al. Aligning large multimodal models with factually augmented rlhf. *arXiv preprint arXiv:2309.14525*, 2023. 1, 2

[28] Hugo Touvron, Thibaut Lavig, Gautier Izacard, Xavier Martinet, Marie-Anne Lachaux, Timothée Lacroix, Baptiste Rozière, Naman Goyal, Eric Hambro, Faisal Azhar, et al. Llama: Open and efficient foundation language models. *arXiv preprint arXiv:2302.13971*, 2023. 2

[29] Chongjun Tu, Peng Ye, Dongzhan Zhou, Lei Bai, Gang Yu, Tao Chen, and Wanli Ouyang. Attention reallocation: Towards zero-cost and controllable hallucination mitigation of mllms. *arXiv preprint arXiv:2503.08342*, 2025. 1, 2

[30] Laurens Van der Maaten and Geoffrey Hinton. Visualizing data using t-sne. *Journal of machine learning research*, 9(11), 2008. 5

[31] Ashish Vaswani, Noam Shazeer, Niki Parmar, Jakob Uszkoreit, Llion Jones, Aidan N Gomez, Łukasz Kaiser, and Illia Polosukhin. Attention is all you need. *Advances in neural information processing systems*, 30, 2017. 1, 3

[32] Chenguang Wang, Xiao Liu, and Dawn Song. Language models are open knowledge graphs. *arXiv preprint arXiv:2010.11967*, 2020. 3

[33] Peng Wang, Shuai Bai, Sinan Tan, Shijie Wang, Zhihao Fan, Jinze Bai, Keqin Chen, Xuejing Liu, Jialin Wang, Wenbin Ge, et al. Qwen2-vl: Enhancing vision-language model's perception of the world at any resolution. *arXiv preprint arXiv:2409.12191*, 2024. 1

[34] Yongxin Wang, Meng Cao, Haokun Lin, Mingfei Han, Liang Ma, Jin Jiang, Yuhao Cheng, and Xiaodan Liang. Eaco: Enhancing alignment in multimodal llms via critical observation. *arXiv preprint arXiv:2412.04903*, 2024. 1, 2

[35] Sangmin Woo, Donguk Kim, Jaehyuk Jang, Yubin Choi, and Changick Kim. Don't miss the forest for the trees: Attentional vision calibration for large vision language models. *arXiv preprint arXiv:2405.17820*, 2024. 1, 2

[36] Ling Yang, Ye Tian, Bowen Li, Xinchen Zhang, Ke Shen, Yunhai Tong, and Mengdi Wang. Mmada: Multimodal large diffusion language models. *arXiv preprint arXiv:2505.15809*, 2025. 1

[37] Hao Yin, Guangzong Si, and Zilei Wang. Clearsight: Visual signal enhancement for object hallucination mitigation in multimodal large language models. In *Proceedings of the Computer Vision and Pattern Recognition Conference*, pages 14625–14634, 2025. 1, 2

[38] Mengxi Zhang, Wenhao Wu, Yu Lu, Yuxin Song, Kang Rong, Huanjin Yao, Jianbo Zhao, Fanglong Liu, Haocheng Feng, Jingdong Wang, et al. Automated multi-level preference for mllms. *Advances in Neural Information Processing Systems*, 37:26171–26194, 2024. 2

[39] Xiaofeng Zhang, Yihao Quan, Chaochen Gu, Chen Shen, Xiaosong Yuan, Shaotian Yan, Hao Cheng, Kaijie Wu, and Jieping Ye. Seeing clearly by layer two: Enhancing attention heads to alleviate hallucination in lylms. *arXiv preprint arXiv:2411.09968*, 2024. 2

[40] Deyao Zhu, Jun Chen, Xiaoqian Shen, Xiang Li, and Mohamed Elhoseiny. Minigpt-4: Enhancing vision-language understanding with advanced large language models. *arXiv preprint arXiv:2304.10592*, 2023. 1